Hindawi
Advances in Civil Engineering
Volume 2022, Article ID 9089652, 13 pages
https://doi.org/10.1155/2022/9089652

Research Article

Stability Analysis of Loess High Slope under Dynamic Compaction Based on Matrix Discrete Element Method

Bingquan Wu,[1,2] **Wankui Ni**,[1,2] **and Haiman Wang**[1,2]

[1]*College of Geological Engineering and Geomatics, Chang'an University, Xi'an 710054, China*
[2]*Key Lab of Western Geological Resources and Geoengineering Under Ministry of Education, Chang'an University, Xi'an 710054, China*

Correspondence should be addressed to Wankui Ni; niwankui@chd.edu.cn

Received 25 April 2022; Revised 22 November 2022; Accepted 7 December 2022; Published 19 December 2022

Academic Editor: Xiao Sun

In order to investigate the safety and stability of loess high slope under dynamic ramming, the MatDem software was used to simulate the process of heavy rammer compacting the spot which was 11 m away from the toe of loess high slope. The rammer was applied with different energies of 10000 kN·m, 8000 kN·m, and 6000 kN·m. In this way, the safety and stability of slope under the action of different dynamic tamping energies can be determined. The results show that the loess high slope presented circular landslide damage by dynamic compaction. Under the same ramming times, with the decrease of ramming energy, the damage degree of loess high slope gradually reduced. According to the displacement value of different monitoring points, the large horizontal and vertical displacement points in landslide were obtained. When the ramming energy was 10000 kN·m and 8000 kN·m, the maximum horizontal displacements were 15.45 m and 10.72 m, and the maximum vertical displacements were 17.43 m and 11.91 m. When the ramming energy was 6000 kN·m, the soil at the bottom of slope would produce slight vibration. Considering the actual project, when the ramming energy was 10000 kN·m and 8000 kN·m, the minimum safe distance was recommended to be 25 m and 20 m. When the ramming energy was 6000 KN·m, the slope remained stable as a whole, and the minimum safe distance suggested should not be less than 11 m. A safety distance of collapse of loess high slope under dynamic compaction was determined, which provided a strong safety guidance for loess high slope construction under dynamic compaction.

1. Introduction

Dynamic compaction method is an effective method to strengthen the foundation, heavy hammer from ten tons to hundreds of tons falls freely from a height of several meters to dozens of meters to tamp soil body. and the requirements of bearing capacity and anti-deformation ability of foundation in engineering construction are met [1]. The dynamic compaction method is mainly suitable for coarse granular soil with particle sizes larger than 0.05 mm, especially for collapsible loess foundation. It has been widely promoted in the Loess Plateau region of Northwest China, such as cutting mountains to make land and increasing land use area. However, the dynamic compaction will have irreversible effects on the surrounding soil and even cause damage to the surrounding slope soil [2], such as slope spalling, small slip collapse, and landslide.

In order to study the destruction of surrounding slope soil by the dynamic compaction method, relevant scholars have carried out research through theoretical analysis, laboratory, field, and model tests [3]. Chow et al. [4] studied the propagation law of dynamic compaction vibration stress wave in soil based on one-dimensional wave equation theory. Jiang et al. [5, 6] studied the stress process of foundation reinforcement by dynamic compaction and analyzed the change process of different types of stress wave and soil stress caused by dynamic compaction. Lee and Gu [7] proposed a method to evaluate the depth and degree of influence of dynamic compaction on sand foundation treatment. Ghassemi et al. [8] established a mathematical

model to analyze the effects of initial density and dynamic compaction energy level on the sand. Wang et al. [9] analyzed the influence of impact load on soil stress and deformation through a dynamic triaxial laboratory test. Arslan et al. [10, 11] analyzed the influence of different rammer shapes on foundation soil. Han et al. [12] used a ramming method with the same energy level, different rammer weight, and falling distance and studied the motion law of the rammer by analyzing the changes in rammer acceleration, velocity, and displacement using the model test. Ali et al. [13, 14] believed that the stability of the slope was related to the geometric shape of the slope and the distance between dynamic load and slope and analyzed the related parameters affecting the safety and stability of the slope. However, laboratory and related model tests cannot fully reflect the problems in practical engineering and only analyze the related mechanical changes and failure forms of soil under dynamic load to a certain extent, which has a certain limitation. Li and He [15] studied the failure mode and dynamic stability of rock slope under earthquake and expounded the failure mechanism of rock slope. For example, in order to obtain real and effective test data, Feng et al. [16] studied the effect of high energy dynamic compaction on collapsible loess through the field test. Fu et al. [17] studied the attenuation law of dynamic compaction vibration and proposed a safety impact distance of dynamic compaction on surrounding buildings. In the case analysis of loess landslide, the factors causing landslide are not only earthquake [18] but also construction machineries, such as vibration of drilling rig [19] and dynamic compaction vibration.

Some researchers have studied the influence of dynamic compaction on surrounding soil by numerical calculation methods, such as finite element method and finite difference method. Elham and Hamidi [20] used ABAQUS FEM to simulate the safe and stable state of the sand slope with different slope angles under dynamic compaction impact load. Abdizadeh et al. [21] performed transverse dynamic compaction of slope based on the principle of soil reinforcement by dynamic compaction, and the ABAQUS FEM was used to simulate the transverse dynamic compaction of the three-dimensional slope model. Giri and Sengupta [22] used FLAC FEM to analyze the slope stability under dynamic compaction after soil nailing support, and the numerical results were close to the experimental results. Chang et al. [23] used the discrete element method to analyze the failure law of loess slope under seismic load. Xue et al. [24] used the discrete element method to establish a 3D discrete element and finite difference coupling model and verified the process of soil dynamic stress propagation through the model impact test. Liu et al. [25] used the discrete element method to effectively simulate the principles of discontinuity, inhomogeneity, and large deformation failure of rock and soil. On the basis of the matrix calculation of the discrete element method, a high-performance MatDEM was developed, and a discrete element simulation of the project scale was realized. Scaringi et al. [26] used PFC and MatDEM as well as MassMov2D and Massflow to conduct a comparative analysis of the process of rock landslide, and the calculation results showed that MatDEM had obvious advantages in imaging of slope landslide movement process. It was close to the actual process of debris flow landslide. Le et al. [27] used MatDEM to conduct discrete element simulation of dry cracking in thin clay layers and more clearly analyzed the development process of the fracture network. Zhang et al. [28] carried out the secondary development of MatDEM software and analyzed the macro and microdeformation and failure of surrounding rock, and the results were close to the engineering practice. Xia et al. [29] used MatDEM to construct a three-dimensional discrete element model to analyze the motion process of high slope landslide and the distance of slope slip. The construction of high-energy dynamic compaction will cause a destructive influence on the loess high slope, so the numerical simulation software used should be able to simulate the destruction process of the loess high slope under dynamic compaction. The discrete element method has obvious advantages over the finite element method and the finite difference method in simulating discontinuity, inhomogeneity, and large deformation failure of soil. The MatDEM uses the matrix discrete element method to realize a application of engineering scale, which can realize a macro and microtransformation of discrete element model, and the final slope failure state calculated is closer to the actual situation.

In engineering practice, dynamic compaction may cause large deformation and even landslide failure of loess high slope. The stability of slope under dynamic load by the propagation mechanism of vibration waves in slope was analyzed by many scholars, but the stability of loess high slope under dynamic compaction was few studied. The finite element method was more used to simulate the stress of slope deformation, but the discrete element method was seldom used to simulate the destruction of the loess high slope by dynamic compaction. There is not a quantitative evaluation for the failure of the loess high slope under ramming, which could not provide a reasonable and accurate safe distance for the construction near the loess high slope. Based on a practical engineering and the mechanism of dynamic compaction energy transmission in the loess high slope, MatDEM software was used to analyze the failure form of loess high slope under dynamic compaction and to quantitatively analyze the vertical and horizontal distance of landslide in this paper. The safe distance of loess high slope collapse under dynamic compaction was determined. It provides a powerful safety guide for compaction engineering of peripheral foundation soil of loess high slope.

2. Engineering Background

This study takes the failure of a high slope around loess foundation of a project site in Shaanxi Province, China as the research object. The ramming position of the project site and the failure of the slope are shown in Figure 1(a), and the gradient and height of the slope are shown in Figure 1(b). According to survey results, the site strata were mainly cultivated soil and eolian loess of the quaternary middle regeneration system, and no groundwater was found within the survey depth. The elevation of the dynamic compaction

construction site was 895 m, the elevation of the surrounding slope top was 945 m, the slope height H was 50 m, the slope Angle α was 60°, and the soil moisture content was 0.16. The dynamic compaction position was about 11 m away from the slope toe. The energy level of dynamic compaction used in site construction was 8000 kN·m. After ramming five times, the soil on the slope surface cracked, and the slope showed integral failure and forward slipped. At the slope toe, some blocks of different sizes were scattered, and soil particles of different sizes were scattered around some stacked blocks. The slump damage of the slope had a severe impact on the safely constructing of subsequent projects and increased the cost of the project.

3. Analysis of Fluctuation Theory

3.1. Damage Mechanism of Dynamic Compaction Vibration Wave to Soil. In the process of dynamic compaction, the gravitational potential energy of the drop hammer, falling from a height, was converted into kinetic energy. When the drop hammer interacted with soil, a part of the kinetic energy was converted into acoustic energy propagating around and thermal energy generated by friction between drop hammer and soil. Most of the kinetic energy was converted into an impact kinetic energy of random free vibration of soil, which propagated in the soil body as a wave system consisting of compression wave, shear wave, and Rayleigh wave, and formed a wave field in foundation (as shown in Figure 2).

According to the propagation properties of wave, Rayleigh waves could carry about 2/3 of the energy, centered in the ramming pit, and propagated around the surface, which caused the surrounding objects to vibrate. During the process of vibration propagation, due to the influence of Rayleigh waves, the surrounding soil produced compression and tension, one part formed extrusion deformation, and the other part formed tensile deformation. Rayleigh waves reached the slope along the surface, caused tensile and extrusion failure of slope soil, and gradually formed a loose layer. Under the action of continuous ramming, the particle connection of the loose layer weakened, constantly fractured, and finally formed exfoliation and collapse of slope soil, which may also form a certain range of serious landslides.

3.2. Computational Analysis. In the context of dynamic compaction numerical simulation, the impact load was calculated using the Scott formula modified by Qian et al. [30]. When ignoring the effect of viscous force on the dynamic response under impact load, the Scott formula could be simplified to the following equation:

$$M\ddot{w} + Sw = 0, \tag{1}$$

where M is the mass of drop hammer, w is the settlement of contact surface, S is the elastic coefficient under loading, $S = 2rE/(1-\nu^2)$, r is the radius of drop rammer, E is elastic modulus, and ν is Poisson's ratio.

According to initial conditions, $w(0) = 0$ and $\ddot{w}(0) = V = \sqrt{2gh}$. where h is the initial height of drop hammer and g is the gravitational acceleration. The differential equation is as follows:

$$\sigma = -\frac{M\ddot{w}}{\pi r^2} = \frac{VS}{\pi r^2 \omega}\sin(\omega t), \tag{2}$$

where $\omega = \sqrt{S/M}$, the impact load duration is t, and $t = \pi/2\omega$.

Combined with the simulated site situation, mechanical parameters of dynamic compaction are shown in Table 1.

4. Experiment Program

4.1. MatDEM Software. MatDEM is a high-performance discrete element software for rock and soil mass developed by Nanjing University. By using the matrix discrete element algorithm and 3D contact algorithm, the efficient discrete element numerical simulation of millions of particles in the university can be realized. The software can iteratively calculate the velocity and displacement of particles through time steps. The acceleration is obtained by force and mass of particle at the current step, after dT time the velocity and displacement of particle in next step are obtained, and in this way, the process of discrete elements iterative calculation is shown in Figure 3.

4.2. Micromechanical Mechanism. In MatDEM, soil particles are composed of many spherical elements which squeeze into each other, as shown in Figure 4. There is a common contact point between two adjacent particles, and the normal force is $F_n = K_n \cdot X_n$, where K_n is the normal stiffness and X_n is the normal relative displacement. X_n is positive when there is no contact between the two particles, and X_n is negative when there is contact and overlap, as shown in Figure 5(a). If the normal relative displacement X_n exceeds the fracture displacement, the normal connection breaks.

The shear stress $F_S = K_s \cdot X_s$, where K_s is the shear stiffness and X_s is the relative tangential displacement, as shown in Figure 5(b). If the shear force exceeds the ultimate shear stress $F_{S\max}$, the tangential connection breaks. $F_{S\max} = F_{So} - \mu_p F_n$, where F_{So} is the initial shear strength and μ_p is the coefficient of friction between particles. In soil, due to the randomness of normal and tangential connections, when F_n or F_S exceed the corresponding limits, the connection between particles breaks.

The model obeies the Mohr-Coulomb breach criterion. $\tau_n = c + \sigma_n \tan\varphi$, $F_{S\max} = \tau_n$, $c = F_{So}$, $\mu_p = \tan\varphi$, $F_n = \sigma_n$. The relevant parameters in MatDEM are as follows:

$$\begin{aligned}
K_n &= \frac{\sqrt{2}Ed}{4(1-2\nu)},\\
K_S &= \frac{\sqrt{2}(1-5\nu)Ed}{4(1+\nu)(1-2\nu)},\\
X_b &= \frac{3K_n + K_S}{6\sqrt{2}K_n(K_n+K_S)} \cdot T_u \cdot d^2,\\
F_{So} &= \frac{1-\sqrt{2}\mu_p}{6} \cdot C_u \cdot d^2,\\
\mu_p &= \frac{2\sqrt{2}+\sqrt{2}I}{2+2I},\\
I &= \left[\left(1+\mu_i^2\right)^{1/2} + \mu_i\right]^2,
\end{aligned} \tag{3}$$

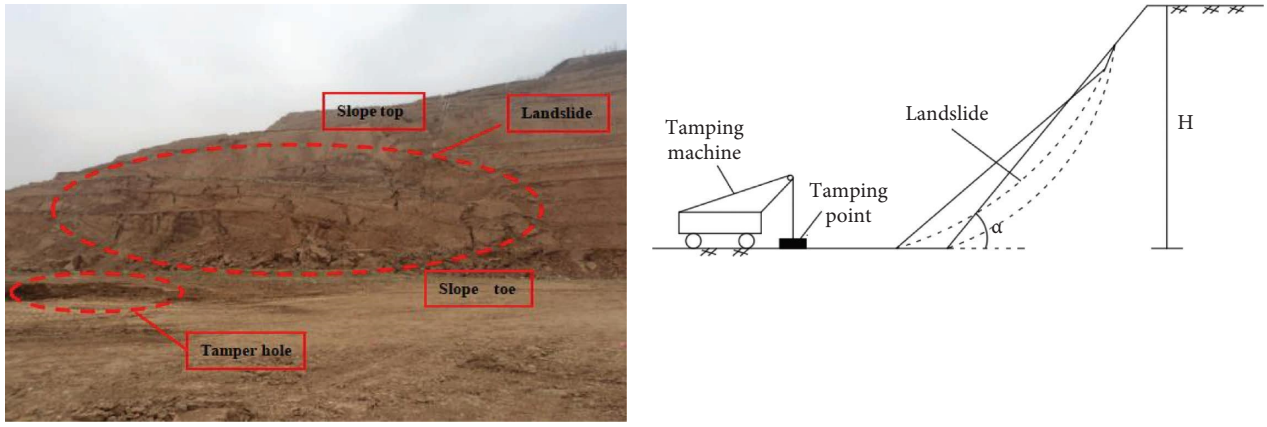

(a) (b)

Figure 1: Destruction site of high slope under dynamic compaction. (a) Actual site drawing. (b) Site location diagram.

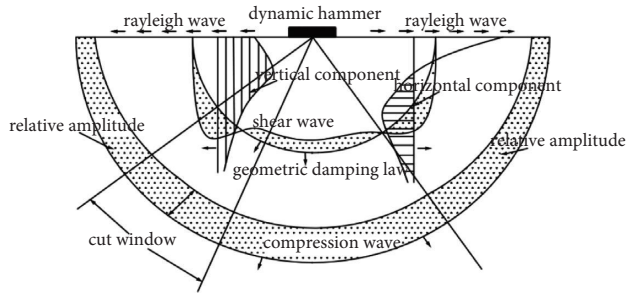

Figure 2: Propagation of shock kinetic energy in soil.

Table 1: Mechanical parameters of dynamic compaction.

Working condition	Ramming energy (kN·m)	Lifted height (m)	Stress amplitude (Pa)	Diameter (m)	Ramming duration	Weight (kg)
1	6000	15	2.01×10^9			
2	8000	20	2.32×10^9	3	0.08	4×10^4
3	10000	25	2.59×10^9			

where X_b is the breaking displacement, T_u is the tensile strength, C_u is the compressive strength, and μ_i is the coefficient of intrinsic friction.

4.3. Experiment Plan. According to the actual situation of the project, the length of a slope numerical model established was 150 m, the height was 80 m, the height difference between the top and toe of the slope was 50 m, the slope angle was 60°, and the soil was assumed to be homogeneous loess. During the dynamic compaction simulation, the drop hammer falled freely from different heights, such as 15 m, 20 m, and 25 m. The distance between the drop hammer and the slope toe was 11 m. Monitoring points were set along the slope from the top to the toe of slope, which were *A*, *B*, *C*, *D*, *E*, *F*, *G*, *H*, and *I*, and the horizontal projection distance of adjacent monitoring points was 3 m, as shown in Figure 6. The macro and microparameters of soil layer were shown in Table 2.

4.4. Calculation Process. After a slope modeling was completed, the soil particles were compacted, and the initial in-situ stress was calculated in the model. After compaction, the compression shape of soil particles was consistent with the field. Five uninterrupted rammings were then performed and numerically calculated. After the fifth rammings were completed, the slope stability was calculated until reaching a new stability after the landslide. Finally, the test results were exported and sorted, as shown in Figure 7.

5. Results and Discussion

5.1. Influence of Different Tamping Energies on Slope. In this study, various ramming energies of 10000 kN·m, 8000 kN·m, and 6000 kN·m were used to strike the slope at a distance of 11 m from slope toe. The deformations of the slope at the first, second, third, fourth, and fifth rammings were recorded. After the ramming was completed, a landslide

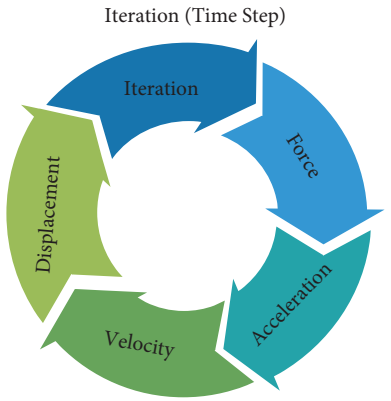

Figure 3: Time step iteration loop.

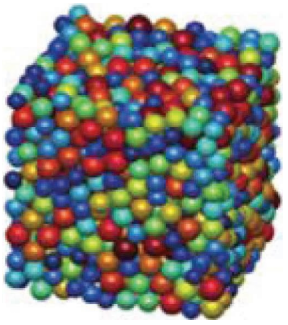

Figure 4: Soil model.

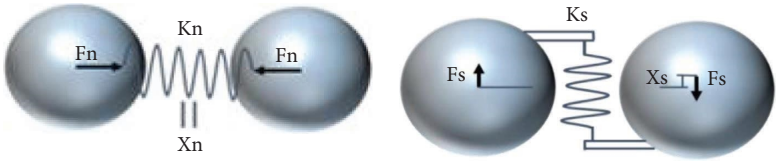

Figure 5: Contact model of adjacent soil elements. (a) Compression. (b) Shear.

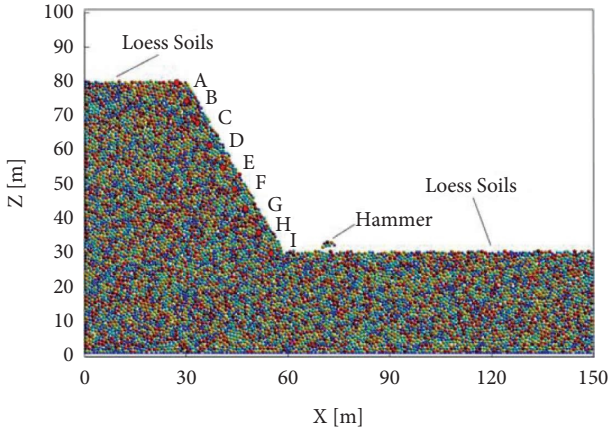

Figure 6: Two-dimensional numerical model.

Table 2: Macro and micromechanical parameters of soil layer.

Macromechanical parameters					Micromechanical parameters				
Elastic modulus E/(GPa)	Poisson's ratio λ	Tensile strength T_u /(MPa)	Compressive strength C_u/(MPa)	Internal friction coefficient u_i	Normal stiffness K_n /(kN·m^{-1})	Tangential stiffness K_s /(kN·m^{-1})	Fracture displacement X_b/(m)	Shear resistance F_{so}/(kN)	Friction coefficient μ_p
5	0.35	0.02	0.3	0.55	2.34×10^4	0.4×10^4	1.29×10^{-5}	6.73	0.16

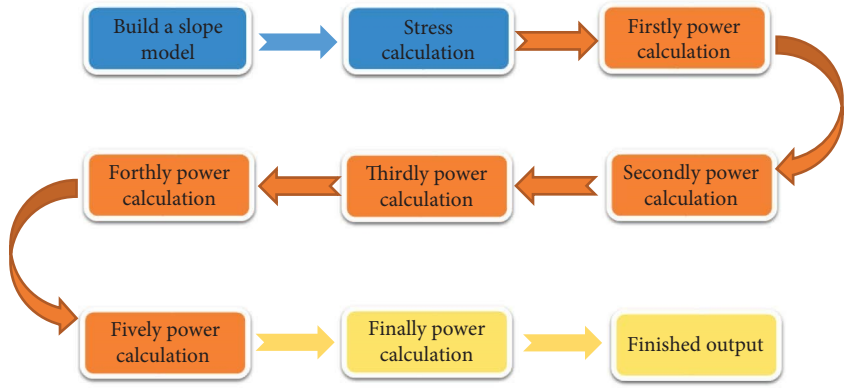

Figure 7: Schematic diagram of calculation flow.

dynamic calculation was carried out on the slope body. Finally, the results were output, as shown in Figure 8.

The drop hammer was 11 m away from slope toe, and the lifting height was 25 m. After free falled, the drop hammer hitted the ground, and the slope suffered a tamping energy of 10000 kN·m. After the first ramming, it can be seen that there was microvibration on the slope (Figure 8(a)). After the second ramming, a relatively obvious fracture surface appeared at a distance of 20 m from slope toe (Figure 8(b)). After the third and fourth rammings, the fracture surface further extended along the height of slope (Figure 8(c) and Figure 8(d)). Finally, after the fifth ramming, the fracture surface penetrated to the slope top, forming a obvious arc sliding surface, and causing the slope to be about to collapse (Figure 8(e)). When the slope exceeded the original limit stable state, a fracture surface slip occurred, and then, a new stability after slipping was reached (Figure 8(f)).

The drop hammer was 11 m away from slope toe, and the lifting height was 20 m. After free falled, the drop hammer hitted the ground, and the slope suffered a tamping energy of 8000 kN·m. After the first and second rammings, the slope appeared microvibration, and the impact of ramming on the slope was weak (Figures 9(a) and 9(b)). After the third ramming, there were clear microcracks on the slope surface at 15 m from the slope toe (Figure 9(c)). After the fourth ramming, there was an obvious circular landslide surface in slope surface (Figure 9(d)). After the fifth ramming, the arc fracture surface on the slope was more obvious, but the fracture surface did not penetrate through the slope top (Figure 9(e)). When the slope exceeded the original limit stable state, a fracture surface slip occurred, and then, a new stability after slipping was reached (Figure 9(f)).

The drop hammer was 11 m away from slope toe, and the lifting height was 15 m. After free falled, the drop hammer hitted the ground, and the slope suffered a tamping energy of 6000 kN·m. According to the simulation results, after five consecutive rammings, in addition to 8 m vertical distance from the slope toe, soil particles slided on the slope surface, and it was found that the slope remained stable in general (Figures 10(a)–10(f)).

5.2. Analysis of the Soil Landslide Process at Different Locations. In order to quantitatively analyze the stability state of the slope, various monitoring points were arranged along the slope surface. The points from the top to toe of slope were *A*, *B*, *C*, *D*, *E*, *F*, *G*, *H*, and *I*. The horizontal projection distance between two adjacent monitoring points was 3 m. Based on calculation results, the displacement values in the *X* and *Z* directions of different monitoring points under the action of different ramming energies were obtained to quantitatively analyze the process of landslide sliding.

It can be seen that when the slope suffered a ramming energy of 10000 kN·m, the horizontal and vertical displacements of soil at different locations were shown in Figure 11. With the increase of ramming times, the horizontal sliding distance of each monitoring point increased continuously, and the slope soil had already slipped when fifth ramming were completed. According to the calculation results, when the soil reached a stable state, the horizontal sliding distance of *F* point was the largest, which was 15.45 m. The vertical height of point *F* was 48.75 m, which was located below the midpoint of slope, consistent with the

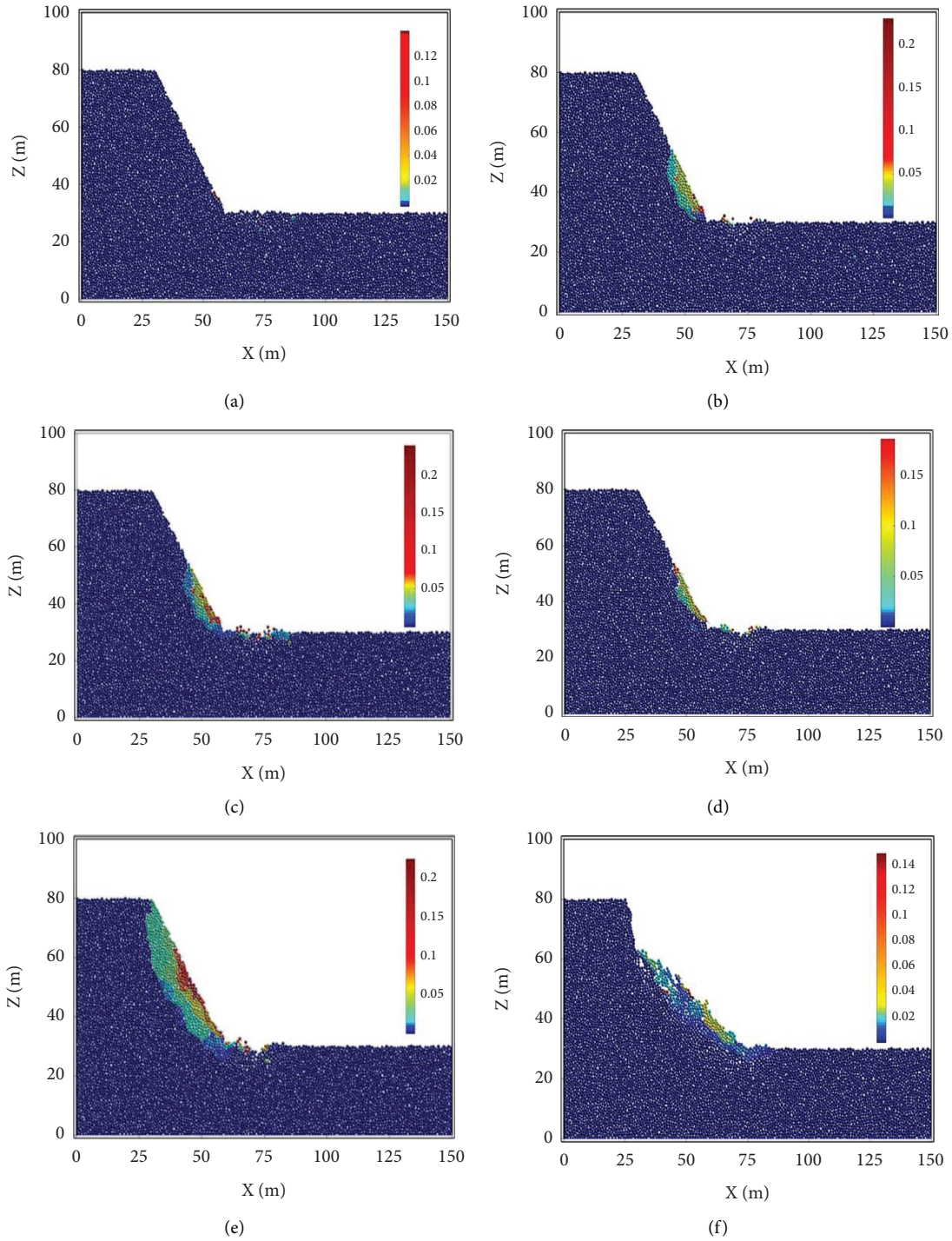

Figure 8: The effects of different ramming times on slope under the tamping energy of 10000 kN·m. (a) The first time ramming; (b) the second time ramming; (c) the third time ramming; (d) the fourth time ramming; (e) the fifth time ramming; (f) the failure state of slope.

actual running state of landslide. The horizontal sliding distance of point G was 14.22 m, and G point had a vertical height of 42.5 m, which was below point F. The horizontal sliding distance of point E was 11.92 m, and E point had a vertical height of 55 m, which was above point F. The horizontal sliding distances of other points were shown in Figure 11(a). Therefore, when the ramming energy acting on the slope was 10000 KN·m and the slope angle was 60°, the 1.5 times maximum horizontal sliding distance in slope monitoring points was recommended as the minimum distance from the slope toe to the machinery or personnel of dynamic compaction construction. Considering the actual project, the minimum safe distance was recommended to be 25 m.

With the increase of ramming times, the vertical sliding distance of each monitoring point increased continuously,

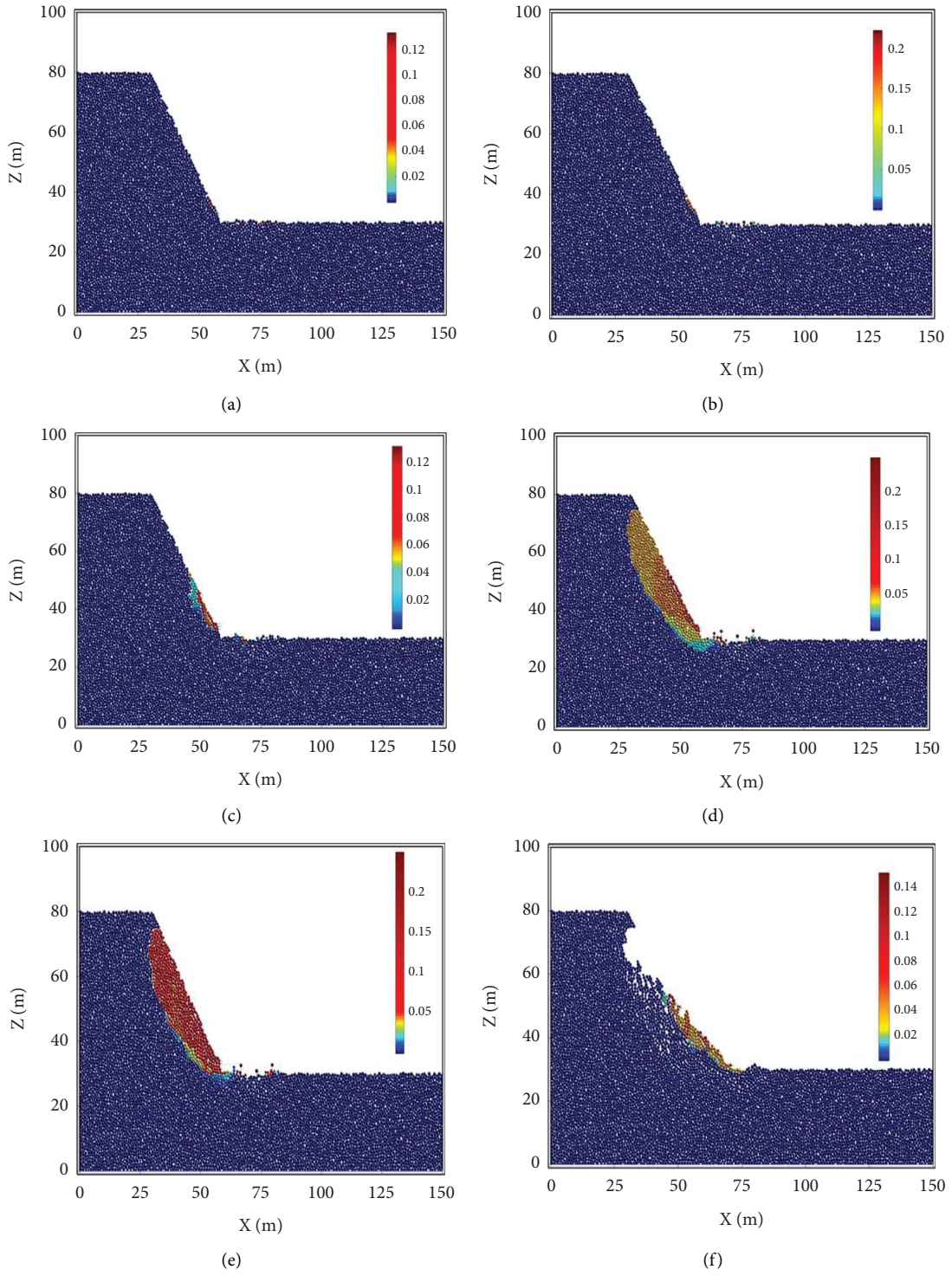

Figure 9: The effects of different ramming times on slope under the tamping energy of 8000 kN·m. (a) The first time ramming; (b) the second time ramming; (c) the third time ramming; (d) the fourth time ramming; (e) the fifth time ramming; (f) the failure state of slope.

and the slope soil had already slipped when fifth ramming was completed. When the slope reached a stable state, the vertical falling distance of point B below the highest point A was the largest, which was 17.43 m. The vertical height of point B was 73.75 m. In the soil particles falling, the particles on the slope surface first falled while the particles at the bottom of slope reached the level ground in advance. Particles in the upper part of slope were hindered by the particles which had reached the ground earlier, and the slipping speed of the particles in the upper part gradually decreased. However, the horizontal and vertical displacements of particles gradually increased until moving forward

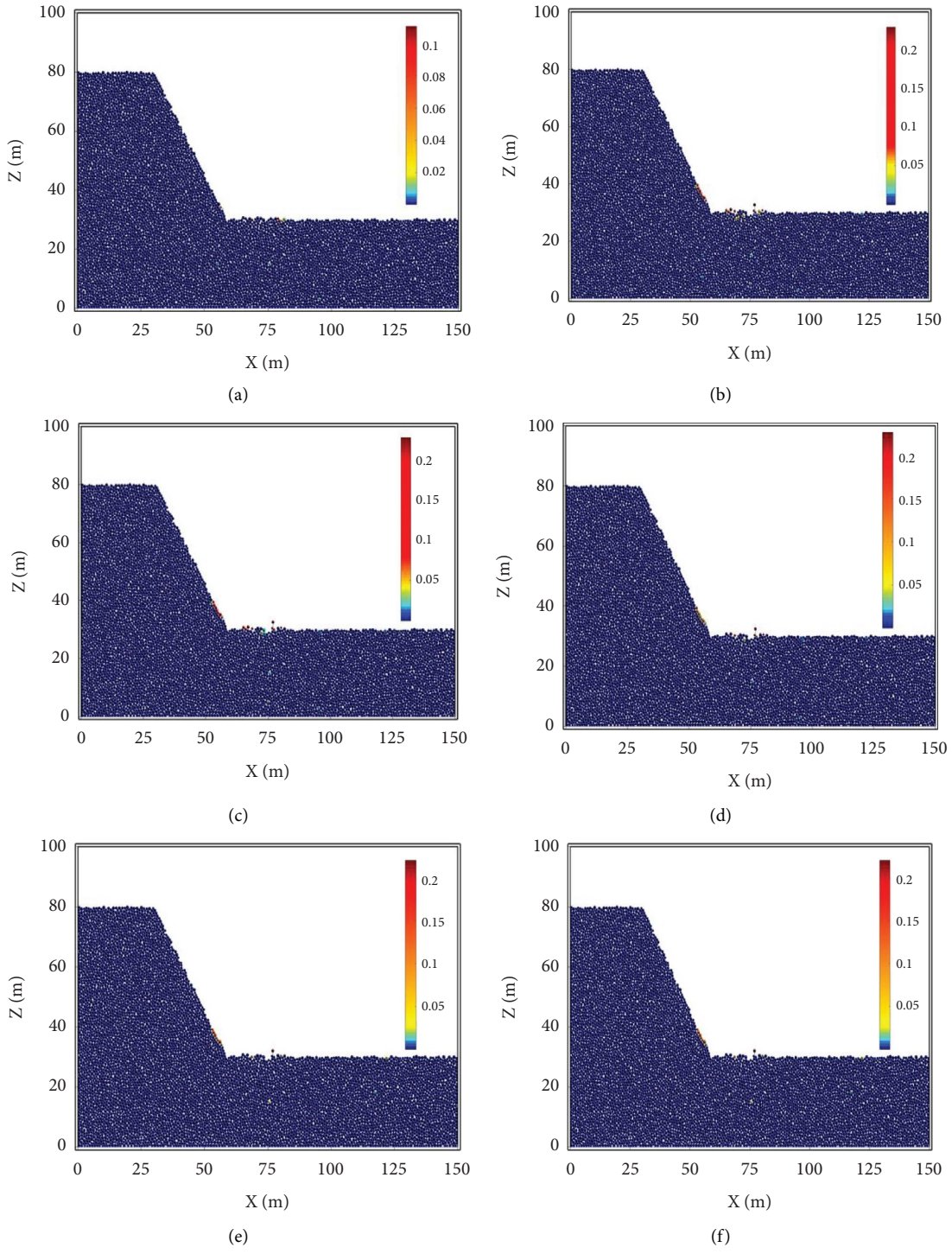

Figure 10: The effects of different ramming times on slope under the tamping energy of 6000 kN·m. (a) The first time ramming; (b) the second time ramming; (c) the third time ramming; (d) the fourth time ramming; (e) the fifth time ramming; (f) the failure state of slope.

and falling at zero velocities. The vertical drop distances of other points were shown in Figure 11(b).

When the slope suffered a ramming energy of 8000 kN·m, the horizontal and vertical displacements of soil at different locations were shown in Figure12. With the increase of ramming times, the horizontal sliding distance of each monitoring point increased continuously, and the slope soil had already slipped when fifth ramming was completed. According to the calculation results, after the soil reached a stable state, the horizontal sliding distance of point E was the largest, which was 10.72 m. The vertical height of point E was 55 m. The horizontal sliding distance of point G was 10.19 m, and the vertical height of point G was 42.5 m. The horizontal sliding distance of point F was 10.04 m, and the

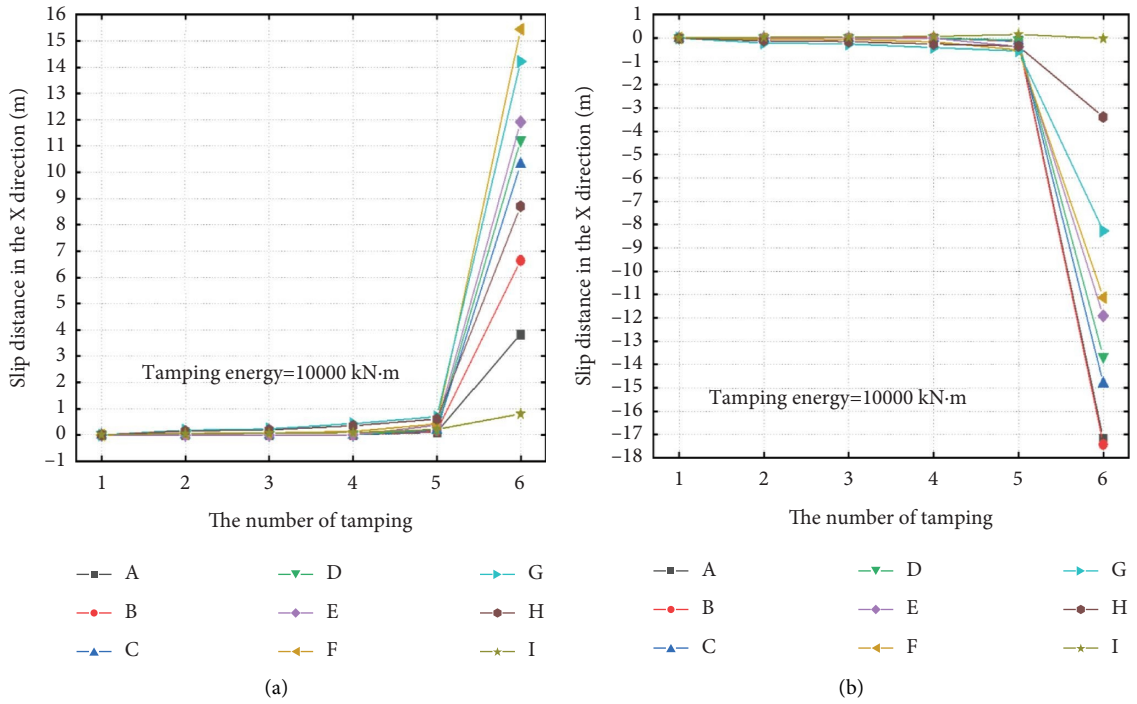

Figure 11: Horizontal and vertical displacements of soil at different positions under the action of 10000 kN·m. (a) Horizontal displacement and (b) vertical displacement.

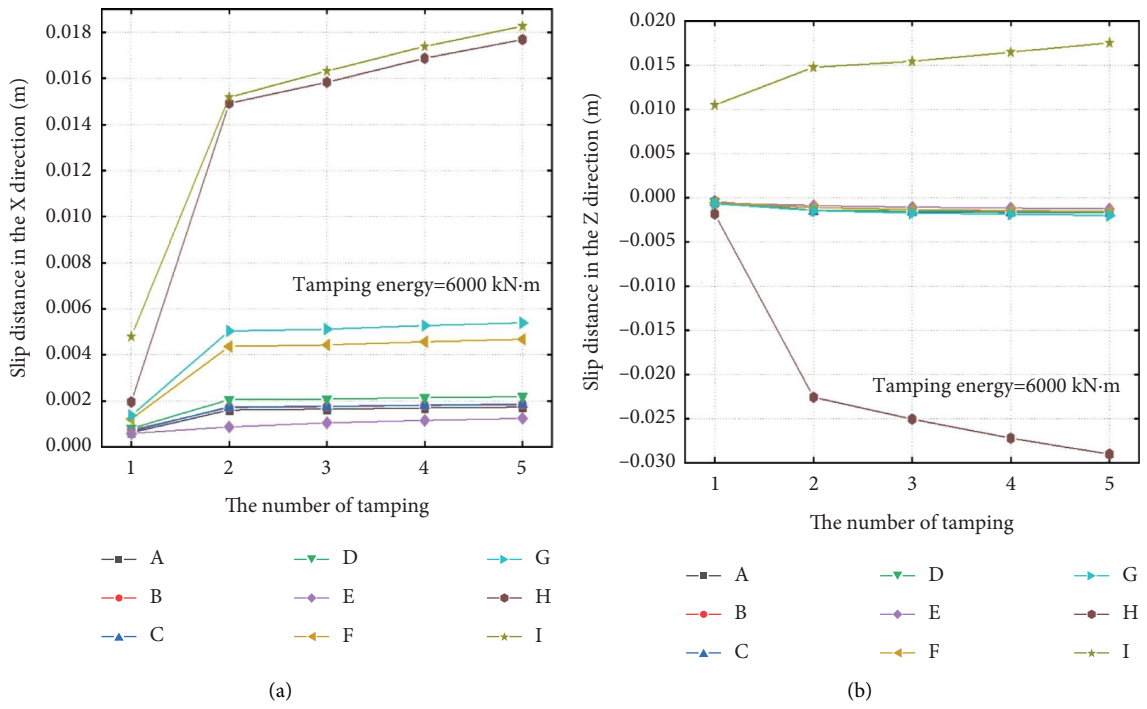

Figure 12: Horizontal and vertical displacements of soil at different positions under the action of 6000 kN·m. (a) Horizontal displacement and (b) vertical displacement.

vertical height of point F was 48.75 m. The horizontal sliding distances of other points were shown in Figure 13(a). Therefore, when the ramming energy acting on the slope was 8000 KN·m and the slope angle was 60°, the 1.5 times maximum horizontal sliding distance in slope monitoring points was recommended as the minimum distance from the

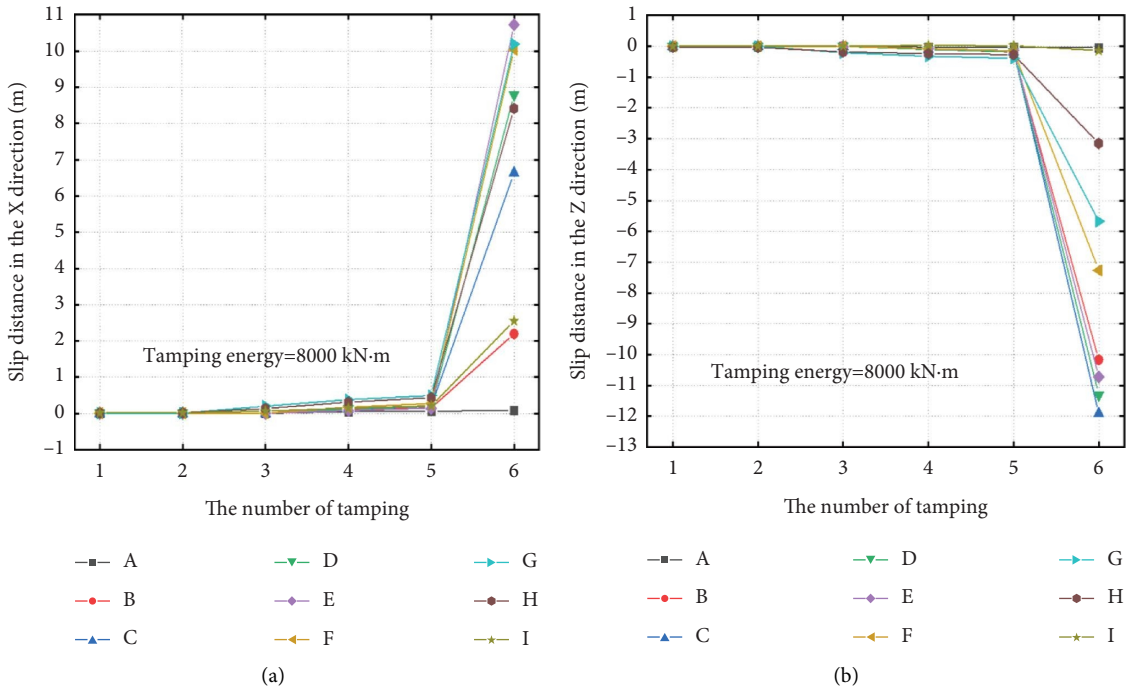

Figure 13: Horizontal and vertical displacements of soil at different positions under the action of 8000 kN m. (a) Horizontal displacement and (b) vertical displacement.

slope toe to the machinery or personnel of dynamic compaction construction. Considering the actual project, the minimum safe distance was recommended to be 20 m.

The vertical drop distance of each monitoring point increased with the increase of ramming times. When the fifth ramming was completed, the slope soil had already fallen. When the slope reached a stable state, the vertical falling distance of point C was the largest, which was 11.91 m. The vertical height of point C was 67.5 m. The vertical drop distance of point D was 11.31 m, and the vertical height of point D was 61.25 m. The vertical drop distances of other points are shown in Figure 13(b).

When the slope suffered a ramming energy of 6000 kN·m, the horizontal and vertical displacements of soil at different locations are shown in Figure 12. After five consecutive rammings, the horizontal sliding distance and vertical falling distance of each monitoring point were very small. The horizontal sliding distance of point I at the bottom of slope was the largest, which was only 1.8 cm. The horizontal sliding distance of the H point was 1.7 cm. The horizontal sliding distances of other monitoring points were less than 0.5 cm, as shown in Figure 12(a). Therefore, when the ramming energy acting on the slope was 6000 KN·m and the slope angle was 60°, the slope remained stable as a whole. According to the distance between dynamic compaction machine and slope toe in the established numerical model, it was suggested that the minimum safe distance should not be less than 11 m.

After five consecutive rammings, the vertical sliding distance of point I at the bottom of slope was the largest, which was only 1.8 cm. The vertical sliding distance of the H point was −2.9 cm. It showed that the particles vibrate upward and did not return to the original position under the action of vibration. It was related to the principle of ramming vibration wave propagation, which was consistent with the actual situation. The vertical displacements of other points were small and could be ignored, as shown in Figure 12(b). It could be judged that when the ramming energy was 6000 kN·m, the soil at the bottom of slope which was about 5 m from the slope toe would vibrate slightly, and there would be intermittent falling phenomenon of slope soil particles. However, the entire slope remained safe and stable.

6. Conclusions

Combined with a construction project, the influence of dynamic compaction on the stability of high loess slopes was analyzed, which takes into account the different ramming energies in this paper. The horizontal and vertical displacements of the key monitoring points of slope were calculated and analyzed. The key conclusions are as follows:

(1) According to the engineering practice and numerical simulation results, when a high energy rammer was used, the loess high slope in surrounding mainly exhibited circular landslide failure.

(2) The point with largest horizontal and vertical displacements in landslide was located in the middle of slope. It shows that the soil particles in the middle position of slope increased by the compression force of upper soil particles. Lower soil particles released space which increased the speed of the soil particles

in the middle position of slope. The forward movement and falling distance of intermediate position points were the largest.

(3) Combined with the actual engineering background, at a slope angle of 60°, when the ramming energy acting on the slope was 10000 kN·m and 8000 kN·m, the 1.5 times maximum horizontal sliding distance in slope monitoring points was recommended as the minimum distance from the slope toe to the machinery or personnel of dynamic compaction construction. Considering the actual project, the minimum safe distance was recommended to be 25 m and 20 m. When the ramming energy acting on the slope was 6000 KN·m, the slope remained stable as a whole, and it was suggested that the minimum safe distance should not be less than 11 m.

Data Availability

The data used to support the findings of this study are available from the corresponding author upon request.

Conflicts of Interest

The authors declare that there are no conflicts of interest regarding the publication of this article.

Acknowledgments

This study was financially supported by the National Nature Science Foundation of China (Grant no. 41931285) and the Key Research and Development Program of Shaanxi Province (Grant no. 2020SF-436).

References

[1] X. J. Lv, X. N. Gong, and J. G. Li, "Analysis and research on construction parameters of dynamic compaction," *Rock and Soil Mechanics*, vol. 9, pp. 1628–1632, 2006.

[2] C. M. Gong, Q. G. Cheng, and Z. P. Liu, "Model test study of dynamic responses of loess slope by dynamic compaction," *Rock and Soil Mechanics*, vol. 32, no. 7, pp. 2001–2006, 2011.

[3] M. Pourjenabi, A. Hamidi, and A. M. Asce, "Numerical modeling of dynamic compaction considering critical distance from adjacent structures," *Advances in Soil Dynamics and Foundation*, vol. 240, pp. 79–106, 2014.

[4] Y. K. Chow, D. M. Yong, K. Y. Yong, and S. L. Lee, "Dynamic compaction analysis," *Journal of Geotechnical Engineering*, vol. 118, no. 8, pp. 1141–1157, 1992.

[5] P. Jiang, R. Q. Li, and D. F. Kong, "Analysis of large deformation collision in dynamic compaction," *Chinese Journal of Geotechnical Engineering*, vol. 2, pp. 222–226, 2000.

[6] W. H. Shui, T. H. Wang, and Y. L. Wang, "Analysis of the impact stress during dynamic compaction on collapsible loess," *Building Science*, vol. 1, pp. 33–36, 2003.

[7] F. H. Lee and Q. Gu, "Method for estimating dynamic compaction effect on sand," *Journal of Geotechnical and Geoenvironmental Engineering*, vol. 130, no. 2, pp. 139–152, 2004.

[8] A. Ghassemi, A. Pak, and H. Shahir, "Validity of Menard relation in dynamic compaction operations," *Proceedings of the Institution of Civil Engineers - Ground Improvement*, vol. 162, no. 1, pp. 37–45, 2009.

[9] N. Q. Wang, X. L. Liu, B. Han, and B. T. Liu, "Test of dynamic strength characteristics of lishi loess," *Applied Mechanics and Materials*, vol. 303-306, no. 303, pp. 2902–2907, 2013.

[10] H. Arslan, G. Baykal, and O. Ertas, "Influence of tamper weight shape on dynamic compaction," *Proceedings of the Institution of Civil Engineers - Ground Improvement*, vol. 11, no. 2, pp. 61–66, 2007.

[11] S. Kundu and B. V. S. Viswanadham, "Studies to evaluate the impact of tamper on the depth of improvement in dynamic compaction," *Japanese Geotechnical Society Special Publication*, vol. 2, no. 59, pp. 2033–2037, 2016.

[12] Y. S. Han, Y. L. Tong, and X. H. Bai, "Model test on process of hammer under dynamic compaction of loess," *Chinese Journal of Rock Mechanics and Engineering*, vol. 34, no. 3, pp. 631–638, 2015.

[13] M. Ali, "Impact of model scale on the results of dynamic compaction adjacent to the sandy slopes," *Proceedings of the Institution of Civil Engineer-Ground Improvement*, vol. 172, no. 2, pp. 1–11, 2018.

[14] A. Vahidipour, A. Ghanbari, and A. Hamidi, "Experimental study of dynamic compaction adjacent to a slope," *Proceedings of the Institution of Civil Engineers - Ground Improvement*, vol. 169, no. 2, pp. 79–89, 2016.

[15] Y. Li and C. M. He, "Research progress on dynamic stability of layered rock slope," in *Proceedings of the IOP Conference Series: Earth and Environment Science*, vol. 760, no. 1, Article ID 012058, Suzhou, China, March 2021.

[16] S. J. Feng, F. L. Du, Z. M. Shi, W. H. Shui, and K. Tan, "Field study on the reinforcement of collapsible loess using dynamic compaction," *Engineering Geology*, vol. 185, pp. 105–115, 2015.

[17] S. F. Fu, L. F. Wu, H. Gao, and X. Liu, "Experimental study of dynamic compaction vibration on the surrounding buildings," in *Proceedings of the AIP Conference Proceedings*, vol. 1820, no. 1, Article ID 060013, Clermont-Ferrand, France, March 2017.

[18] S. B. Zhu, Y. L. Shi, M. Lu, and F. Xie, "Dynamic mechanisms of earthquake-triggered landslides," *Science China Earth Sciences*, vol. 56, no. 10, pp. 1769–1779, 2013.

[19] J. Si-yi, L. Hai-liang, W. Fu, and L. Chun-ling, "Characteristics and mechanism of loess landslide induced by drill vibration," in *Proceedings of the IOP Conference Series: Earth and Environmental Science*, vol. 304, no. 4, Article ID 042003, Boston, MA, USA, June 2019.

[20] G. Elham and A. Hamidi, "Improvement parameters in dynamic compaction adjacent to the slopes," *Journal of Rock Mechanics and Geotechnical Engineering*, vol. 7, no. 2, pp. 233–236, 2015.

[21] D. Abdizadeh, M. S. Pakbaz, and B. Nadi, "Numerical modeling of lateral dynamic compaction on the slope in dry sand," *KSCE Journal of Civil Engineering*, vol. 25, no. 2, pp. 398–403, 2020.

[22] D. Giri and A. Sengupta, "Dynamic behavior of small scale nailed soil slopes," *Geotechnical & Geological Engineering*, vol. 27, no. 6, pp. 687–698, 2009.

[23] W. B. Chang, P. Wang, A. G. Xing, H. Wang, Y. Yu, and X. Li, "Failure mode and dynamic response of loess slopes with tectonic joints under seismic action," *Environmental Earth Sciences*, vol. 80, no. 16, p. 531, 2021.

[24] J. Xue, M. Jia, B. Liu, and G. Ma, "Coupled three-dimensional discrete element–finite difference simulation of dynamic

compaction," *Acta Geotechnica*, vol. 16, no. 3, pp. 731–747, 2020.

[25] C. Liu, H. Liu, and H. Y. Zhang, "MatDEM-fast matrix computing of the discrete element method," *Earthquake Research Advances*, vol. 1, no. 3, Article ID 100010, 2021.

[26] G. Scaringi, X. Fan, Q. Xu et al., "Some considerations on the use of numerical methods to simulate past landslides and possible new failures: the case of the recent Xinmo landslide (Sichuan, China)," *Landslides*, vol. 15, no. 7, pp. 1359–1375, 2018.

[27] T. C. Le, C. Liu, C. S. Tang, X. Y. Zhang, and B. Shi, "Numerical simulation of desiccation cracking in clayey soil using a multifield coupling discrete-element model," *Journal of Geotechnical and Geoenvironmental Engineering*, vol. 148, no. 2, Article ID 04021183, 2022.

[28] Z. Z. Zhang, Y. X. Niu, X. J. Shang, R. Zhou, X. Liu, and F. Gao, "Effect of confining pressureon mechanical and energy conversion properties of gas-containing coal under loads," *Geofluids*, vol. 2022, Article ID 3074156, 2022.

[29] G. Q. Xia, C. Liu, C. Xu, and T. Le, "Dynamic analysis of the high-speed and long-runout landslide movement process based on the discrete element method: a case study of the shuicheng landslide in guizhou, China," *Advances in Civil Engineering*, vol. 2021, Article ID 8854194, 2021.

[30] J. H. Qian, X. D. Qian, and W. B. Zhao, "Theory and practice of dynamic consolidation," *Chinese Journal of Geotechnical Engineering*, vol. 6, pp. 1–17, 1986.